Propagation and Reflection of Internal Waves

B. R. Sutherland[a)]
Department of Mathematical Sciences, University of Alberta
Edmonton, AB T6G 2G1, Canada

(Submitted 12 June 1998)

Fully nonlinear numerical simulations are performed to examine the behaviour of large-amplitude internal gravity waves incident upon a level where the Doppler-shifted frequency of the waves is comparable with the background buoyancy frequency. Although linear theory predicts that the waves should reflect if the Doppler-shifted frequency is greater than the buoyancy frequency, it is found that nonlinear effects may greatly enhance the transmission of a wavepacket across a reflecting level. If the Doppler-shifted frequency is moderately less than the buoyancy frequency, then nonlinear effects may greatly enhance the reflection of waves. A range of simulations is performed to characterise the reflection coefficient as a function of the amplitude and spatial extent of the wavepacket. In comparison with horizontally periodic wavepackets, it is found that the nonlinearly enhanced transmission of wavepackets is more significant if they are horizontally compact. This occurs because the wave-induced mean-flow effectively increases and decreases the horizontal phase speed of the waves on the incident and trailing flank of the wavepackets, respectively, and this significantly broadens the frequency spectrum of the waves.

I INTRODUCTION

An internal wave is a disturbance propagating under the effects of buoyancy in a fluid whose density varies with height. These waves are known to transport momentum and energy vertically through the atmosphere and ocean, and they may constitute a significant source of drag to the mean-flow at levels where they break or dissipate. A great number of studies have been devoted to understanding the behaviour of internal waves as they approach a level where the mean-flow speed is comparable with the horizontal phase speed of the waves (*e.g.* Bretherton[1], and recently Winters and D'Asaro[2], Lombard and Riley[3]. Also see Lighthill[4] §4). This is known as the "critical level". In theory and as numerical simulations demonstrate, as internal waves approach a critical level their vertical wavelength decreases to infinitesimal size and their amplitude increases. Eventually, the waves either dissipate or break, and deposit momentum to the mean-flow. If, as is often the case for topographically generated waves, the horizontal phase speed of the waves is less than the mean flow speed, then a drag is exerted on the mean flow near the critical level.

Less well studied is the circumstance in which internal waves encounter a level where the density is almost uniform. In this case, the waves are expected to reflect. More generally, waves are assumed to reflect from a level where their Doppler-shifted frequency equals the background buoyancy frequency[1,5,6]. This is referred to hereafter as a "reflecting level", which is distinct from a critical level. In theory, as internal waves approach a reflecting level, their vertical wavelength increases. Beyond the reflecting level the waves are evanescent, their amplitude decreasing exponentially with distance from the level. Rigourously, the structure of an internal wave at a reflecting level – a "caustic" – is given by linear theory in terms of an Airy function[4]. Linear theory assumes that the waves are monochromatic and small-amplitude. The theory may be applied to small-amplitude wavepackets with a broad frequency spectrum, by applying the superposition principle. However, the behaviour of large-amplitude internal waves at a reflecting level is not so well understood.

Here we examine the transmission and reflection of internal waves across a reflecting level by way of numerical simulations employing the fully nonlinear equations of motion. This work is a continuation of the studies by Sutherland[7] who examined the propagation in non-uniformly stratified stationary flow of horizontally periodic internal waves incident upon a level where the background buoyancy frequency is comparable with the frequency of the incident waves. Therein it was shown that for vertically compact wavepackets, depending on whether the stratification decreases greatly or moderately at a given level, weakly nonlinear effects act either to enhance or diminish, respectively, the transmission of internal waves into regions where the buoyancy frequency is small.

The weakly nonlinear effects are related to what has been called the "self-acceleration" of internal waves (*e.g.* see Grimshaw[8], Fritts and Dunkerton[9]). For a horizontally periodic, vertically compact wavepacket, its phase speed changes due to wave, mean-flow interactions[7]. For example, consider an upward propagating wavepacket whose amplitude decreases with height. At the leading edge of the wavepacket the mean-flow accelerates due to the divergence of its associated momentum flux. If the waves are of large amplitude, the acceleration may be sufficiently large that the wave-induced mean-flow is compa-

a) Fax: (780) 492-6826; phone: (780) 492-0573;
e-mail: bruce.sutherland@ualberta.ca;
web: http://taylor.math.ualberta.ca/~bruce

rable with the horizontal group velocity of the wavepacket. In this case, the horizontal phase speed along the leading edge of the waves increases. Likewise, along the trailing edge of the wavepacket the mean-flow decelerates and the horizontal phase speed of the waves decreases. As a consequence of symmetry, the horizontal wavelength of horizontally periodic waves does not change over time. Therefore as the phase speed of the waves increases and decreases, the frequency increases and decreases, respectively.

In the absence of dissipation, wave breaking or other non-conservative processes, the transient passage of the wavepacket across a fixed vertical level has no permanent effect upon the mean-flow at that point[10,11]. However, the effective changes in the wave frequency due to the self-acceleration of the waves can significantly affect the behaviour of a wavepacket incident upon a reflecting level. Sutherland[7] showed that as a large-amplitude wavepacket approaches a reflecting level the relative changes in the wave frequency become larger. Due to the superposition of the incident and reflecting waves, the amplitude of the disturbance increases by as much as double that of the incident wavepacket. Correspondingly, the changes in phase speed at the reflecting level can be four times as large. These changes can act to enhance the transmission of internal waves across the reflecting level in the following way: as the waves reflect, the frequency of the waves at the trailing edge of the incident wavepacket decreases, and if this reduced frequency is smaller than the buoyancy frequency above the reflecting level, then a propagating wavepacket is transmitted beyond the reflecting level. The wavepacket has larger amplitude than one would predict on the basis of linear transient effects alone.

If no reflecting level exists, weak nonlinearity may nonetheless affect the transmission of internal waves if the buoyancy frequency is comparable to but greater than the Doppler-shifted frequency of the incident wavepacket. In this case, because the phase speed of the waves on the incident flank of the wavepacket increases, the frequency increases. If the buoyancy frequency is smaller than the increased frequency, a proportion of the wavepacket reflects which is larger than that predicted on the basis of linear transient effects.

In this work, we extend these results to consider the behaviour of a wavepacket that is both vertically and horizontally compact, and which is propagating in a uniformly stratified shear flow. A fundamental change in dynamics is expected to occur as a result of the breaking of the horizontal translational symmetry. Whereas a horizontally periodic wavepacket is capable of accelerating the mean-flow either transiently due to wave-wave interactions, or permanently due to wave, mean-flow interactions or dissipation, a horizontally compact wavepacket cannot directly affect the mean-flow. Such a wavepacket is capable of accelerating only the background flow across the extent of wavepacket itself. It is shown that for large-amplitude internal waves this horizontal non-uniformity significantly enhances the wave dispersion. As a result, the frequency spectrum of the wavepacket greatly broadens. As this wavepacket propagates in a shear flow toward a reflecting level, the proportion of the incident wavepacket that is transmitted may be greatly enhanced or diminished.

In section II the details are given of the numerical model used to simulate the propagation of internal waves. Section III first shows the results of simulations of horizontally periodic and horizontally compact wavepackets in uniformly stratified stationary fluid. These control studies demonstrate the effect of self-acceleration upon the wave structure. The results are then shown of simulations of internal waves propagating in uniformly stratified shear flow. The spectra and characteristics of the reflected and transmitted waves are analysed. In section IV, the reflection coefficients are calculated for a range of simulations of small- and large-amplitude wavepackets with different horizontal extents. A summary of these results and their implications to atmospheric and oceanographic modelling are given in section V.

II NUMERICAL MODEL

The propagation of a two-dimensional wavepacket is examined by solving the fully nonlinear, non-hydrostatic equations of motion with specified initial conditions for the wavepacket structure and the background profiles of horizontal velocity $U(z)$ and density $\overline{\rho}(z)$. The numerical model is described in detail in Sutherland[7]; only the salient features are given below. Throughout this paper it is assumed that the flow is uniformly stratified, that is, the background squared buoyancy frequency, $N_\star{}^2 = -(g/\rho_{00})d\overline{\rho}/dz$, is constant. Here g is the gravitational acceleration and ρ_{00} is a reference value of density. The Boussinesq approximation is used, so that the background density profile can be written as $\overline{\rho}(z) = \rho_{00} - \Delta\rho z/H$, in which H is the height of the domain and $\Delta\rho$ ($\ll \rho_{00}$) is the change in density over this height. Characteristic time ($\mathcal{T}$), length ($\mathcal{L}$) and density ($\Delta\rho$) scales are used to express the equations of motion in nondimensional form. The equations for the vorticity, $\zeta = u_z - w_x$, and perturbation density, ρ, fields are

$$\frac{D\zeta}{Dt} = N_0{}^2 \frac{\partial \rho}{\partial x} + \mathcal{D}_\zeta \tag{1}$$

and

$$\frac{D\rho}{Dt} = w + \mathcal{D}_\rho, \tag{2}$$

in which D/Dt is the material derivative, and u and w are the horizontal and vertical velocity fields, respectively. $N_0 = N_\star \mathcal{T}$ is the nondimensional buoyancy frequency. It has been assumed that density fluctuations occur on the scale $\delta\rho = \mathcal{L}\Delta\rho/\mathcal{H}$, in which case ρ is identical to the nondimensional vertical displacement field, ξ. In order to approximate the motion of inviscid waves while keeping the code numerically stable, the diffusion of the vorticity $\mathcal{D}_\zeta$, acts only on scales smaller than the horizontal wavenumber of the wavepacket. On these small length-scales $\mathcal{D}_\zeta = \frac{1}{\mathrm{Re}}\nabla^2\zeta$. Likewise, the diffusion of the perturbation density field acts only on small length-scales in which case $\mathcal{D}_\rho = \frac{1}{\mathrm{Re\ Pr}}\nabla^2\rho$. The Reynolds number is

set to Re = 1000 and the Prandtl number to Pr = 1. Equations (1) and (2) are solved in a horizontally periodic channel with free slip boundary conditions using a mixed spectral-finite difference code developed originally by Smyth and Peltier[12].

The vertical extent of the domain ranges from $-100 \leq z \leq 100$. For horizontally periodic internal waves, the horizontal extent of the domain, L_x, is set to be exactly one wavelength. For horizontally compact wavepackets, the horizontal extent is set to be $L_x = 64\pi \simeq 201$. Typically, this is 10 to 20 times wider than the width of the wavepackets studied. As confirmed by doubling the width of the domain, the periodic boundary conditions have negligible effect upon the evolution of the wavepacket.

The initial wavepacket is vertically localised. Over the extent that the amplitude of the initial wavepacket is non-negligible the background flow is stationary. Explicitly, the initial wavepacket is prescribed in terms of the streamfunction $\psi(x,z)$:

$$\psi(x,z) = \Psi(x,z)\exp[\imath(k_x x + k_z z)] + \ c.c. \tag{3}$$

In simulations of horizontally periodic internal waves, the envelope of the wavepacket is given by

$$\Psi_{\rm PW}(x,z) = A_0 \exp(-|z-z_0|/\sigma_z). \tag{4}$$

In simulations of horizontally compact wavepackets

$$\Psi(x,z) = A_0 \exp(-|z-z_0|/\sigma_z)\exp(-x^2/2{\sigma_x}^2). \tag{5}$$

Here the amplitude is A_0, and σ_x and σ_z are the horizontal and vertical extents, respectively, of the wavepacket. For finite σ_x and σ_z, and small amplitude A_0, the initial wavepacket defined by equation (3) and either (4) or (5) may be thought of as the superposition of monochromatic waves spanning a broad frequency range centred about a frequency ω, determined from the wavenumber vector (k_x, k_z). The frequency ω is to be estimated from the dispersion relationship for internal waves

$$\omega = N_0 k_x / \sqrt{{k_x}^2 + {k_z}^2}. \tag{6}$$

If $1/\sigma_x \ll k_x$ and $1/\sigma_z \ll k_z$ (as is the case in all the studies presented here), the frequency range is sharply peaked about ω and, for a small amplitude wavepacket, linear theory may be applied to it as if it was monochromatic.

The qualitative results presented here are not sensitively dependent upon the form of the wavepacket envelopes given by equations (4) and (3). The vertical structure of the envelope is set to be exponential because this corresponds to the structure of a growing and decaying wavepacket. For horizontally compact wavepackets, the horizontal structure of the envelope is set to be Gaussian in order to be representative of a statistical ensemble of waves with wavenumber spectrum centred k_x.

For simplicity, the length-scale is chosen so that $k_x = 1$ and the time-scale is chosen so that $N_0 = 1$. In the Boussinesq approximation, there is no difference in the behaviour of upward and downward propagating wavepackets. However, to be consistent with studies of internal waves propagating downward from the ocean surface[13], the internal waves are prescribed initially with positive vertical wavenumber so that the waves propagate downward.

Studies are performed only for wavepackets with vertical wavenumber $k_z = \sqrt{2}/2 \simeq 0.71$. This value is chosen because, with $k_x = 1$, periodic internal waves propagate downward with the largest group velocity $c_{gz} = -2/3\sqrt{3} \simeq -0.38$. In this case $\omega = \sqrt{2/3} \simeq 0.82$. From linear theory, an estimate of the initial amplitude of the vertical displacement field is found to be $A_\xi \simeq 2.45 A_0$. Thus with $A_0 = 1$, for example, the maximum initial vertical displacement is approximately 39% of the horizontal wavelength. The vertical extent of the wavepacket is also fixed with $\sigma_z = 5$, so that approximately 1 vertical wavelength spans the depth of the wavepacket. The width σ_x and amplitude A_0 are allowed to vary. As the wavepacket propagates downward into flow moving at speed $U(z)$, linear theory predicts that the waves are Doppler-shifted with frequency $\Omega(z) = \omega - k_x U(z)$.

The background flow is defined by

$$U(z) = U_1[1 - \tanh(z/D)]/2, \tag{7}$$

in which U_1 is the flow speed well below the initial wavepacket and D is the depth over which the background changes from stationary flow above $z = 0$ to flow moving at speed U_1 below $z = 0$. Throughout we set $D = 5$. The wavepacket encounters a reflecting level if U_1 is sufficiently negatively large. Explicitly, this occurs if $U_1 < \sqrt{2/3} - 1 \simeq -0.18$.

The co-ordinate system is chosen so that the flow changes about $z = 0$, and the wavepacket is centered initially about $(x_0, z_0) = (0, 25)$. Thus the wavepacket is sufficiently close to the region where the background flow changes, but the initial wavepacket amplitude near $z = 0$ is negligible.

Typically, simulations are run for times between $t = 0$ and 200. From linear theory, we estimate that the wavepacket propagates a total vertical distance of $z \simeq 76$ at the end of a simulation. Therefore, the vertical extent of the domain is sufficiently large that the wavepacket has negligibly small amplitude near the top and bottom boundaries throughout the simulation.

Figure 1 shows a typical initial condition for the simulations. Figure 1a shows the horizontal velocity profile $U(z)$ with $D = 5$, and $U_1 = -0.2$. In this case, the Doppler-shifted frequency of the wavepacket as it propagates well below $z = 0$ is $\Omega \simeq 1.02$, and therefore a reflecting level exists near $z = 0$ in this case. Figure 1b shows the perturbation density field $\rho(x,z)$ of an initial wavepacket with amplitude $A_0 = 0.04$ and horizontal extent $\sigma_x = 10$. The down and rightward tilt of the phase lines is consistent with the structure of internal waves that propagate downward to the right.

III RESULTS

Here the results are presented of control simulations examining the propagation of wavepackets in uniformly strati-

fied, stationary flow. These simulations serve to demonstrate how nonlinearity affects the propagation and dispersion of the waves. Following this the results are presented of a range of simulations performed to examine the behaviour of internal waves incident upon a level in a background shear flow where $\Omega/N_0 \simeq 1$. The effect of varying the initial amplitude and horizontal extent of the wavepacket is examined.

A CONTROL SIMULATIONS

The effect of nonlinearity upon the dispersion of internal waves is demonstrated by comparing the behaviour of small- and large-amplitude wavepackets. The structure of horizontally periodic wavepackets at time $t = 200$ in a simulation are shown in Figure 2. Figure 2a shows the vertical profile of the Reynolds stress per unit mass, $\tau(z) = \langle u'w' \rangle$, in which u' and w' are the perturbation horizontal and vertical velocities, respectively, and the angle brackets denote the domain horizontal average. The profile is shown for a simulation of a small-amplitude wavepacket with $A = 0.01$. The Reynolds stress is negative over the extent of the wavepacket as expected for a wavepacket that transports forward momentum downward. Figure 2b shows the corresponding perturbation density field, $\rho(x, z)$, at the same time. Although there has been weak wave dispersion, the diagram demonstrates that the extent of the wavepacket and the tilt of the phase lines is approximately the same as those of the initial wavepacket. The centroid position of the wavepacket is calculated from the weighted average of the momentum flux using only values within 95% of the minimum value of τ. The width is the standard deviation of this normalised distribution. At time $t = 0$ the wavepacket is found to be centred at $z = 25.0$, as expected. The width of the wavepacket is 3.7, moderately smaller than the e-folding depth $\sigma_z = 5$. At time $t = 200$ the wavepacket is centred at $z \simeq -47.2$ with width 4.3. According to linear theory, small-amplitude waves are expected to propagate downwards at the speed of the vertical group velocity $c_{gz} \simeq -0.38$. Thus at time $t = 200$ the wavepacket is expected to be localized about $z = -51$, which is moderately deeper than its observed position. This discrepancy occurs because the initial wavepacket, being vertically compact, is the superposition of internal waves with a range of vertical wavelengths centred about $k_z = \sqrt{2}/2$. Thus the wavepacket is expected to propagate with vertical velocity moderately less than c_{gz}.

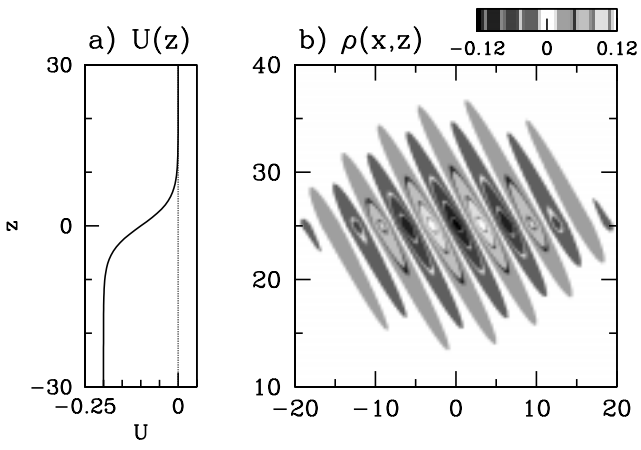

FIG. 1. The a) background horizontal velocity profile and b) perturbation density field of an initial wavepacket in a typical simulation.

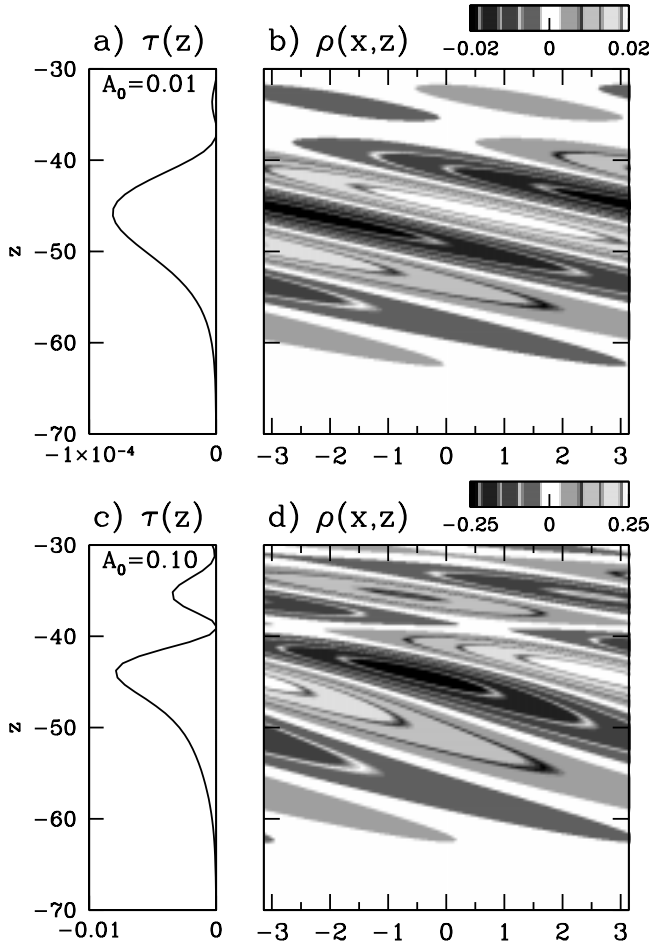

FIG. 2. The a) Reynolds stress profile and b) perturbation density field associated with a horizontally periodic wavepacket with $A_0 = 0.01$ in a control simulation at time $t = 200$. Diagrams c) and d) show the corresponding plots for a wavepacket with $A_0 = 0.10$.

As in Figures 2a and b, Figures 2c and d show the Reynolds stress profile and perturbation density field, respectively, at time $t = 200$ for a simulation of a large-amplitude wavepacket with $A_0 = 0.10$. In this case, the dispersion of the wavepacket is more pronounced. The Reynolds stress profile shows multiple peaks, though the peak at the leading edge is largest. For this leading peak, the centroid position is at $z \simeq -46.5$ and the width of the peak is 4.1. The centroid of the wavepacket including the trailing peaks is at $z \simeq -44.2$ with width 6.1. Thus the effect of weak nonlinearity associated with the large-amplitude wavepacket is to moderately reduce the average vertical speed of propagation of the wavepacket and to en-

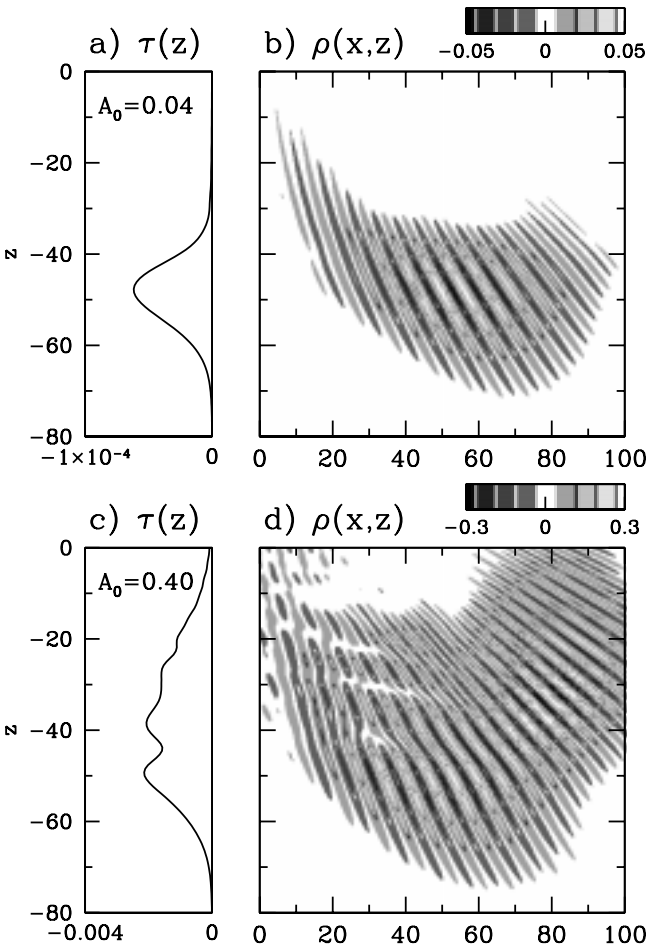

FIG. 3. As in Figure 2 but for compact wavepacket with width $\sigma_x = 10$ and in a) and b) $A_0 = 0.04$, and in c) and d) $A_0 = 0.40$.

hance its dispersion.

In comparison with horizontally periodic wavepackets, simulations have been performed of horizontally and vertically compact wavepackets in uniformly stratified stationary flow. As in Figure 2, Figure 3 shows the Reynolds stress profiles and perturbation density fields at time $t = 200$ taken from simulations of small and large-amplitude wavepackets. The initial horizontal width of both wavepackets is $\sigma_x = 10$. Figures 3a and b show the structure of a small-amplitude wavepacket with $A_0 = 0.04$. The wavepacket undergoes greater dispersion compared with that of the horizontally periodic wavepacket. At time $t = 200$, the peak amplitude of the perturbation density field is $|\rho'| \simeq 0.04$, which is almost one-third the peak amplitude at time $t = 0$. The phase tilt of the waves to the left of the wavepacket centre is more vertical and the phase tilt of the waves to the right is more horizontal. The position of the centroid of the wavepacket at this time is $z \simeq -48.8$ with width 6.6. Thus the wavepacket is approximately 80% wider than the small-amplitude horizontally periodic wavepacket shown in Figure 2b. The average vertical speed is approximately the same in both cases.

Figure 3c shows the Reynolds stress profile and Figure 3d shows the perturbation density field at time $t = 200$ of a large-amplitude wavepacket with $A_0 = 0.40$. The dispersion of the wavepacket is significant in this case. The wavepacket has both broad vertical and horizontal extents. The position of the centroid of the wavepacket is $z \simeq -38.2$ and its width is 14.1. Thus, among other effects, nonlinearity acts to significantly slow the vertical speed of propagation of the wavepacket, and this effect is much more pronounced if the wavepacket is horizontally compact. As discussed below, this is a consequence of the wave-wave interactions that act non-uniformly over the extent of the wavepacket to locally change the phase speed of the waves.

B WAVE SELF-ACCELERATION

The effect of weak nonlinearity upon the spectrum of the wavepacket is shown in Figure 4, which contains contour plots of the normalised power spectrum of the a) small-amplitude ($A = 0.04$) and b) large-amplitude ($A = 0.40$) wavepackets shown in Figures 3b and d, respectively. The power spectrum is computed from the square of the components of the two-dimensional discrete Fourier transforms of the perturbation density fields. The result is normalised by its maximum value. The contours in both figures range from 0.1 to 0.9 by an interval of 0.2. Figure 4a shows that the internal wave spectrum for the small-amplitude wavepacket is sharply peaked about wavenumber vector $(k_x, k_z) \simeq (1.0 \pm 0.06, 0.69 \pm 0.12)$, close to the wavenumber vector, $(1, 0.71)$, prescribed to the wavepacket at time $t = 0$. The horizontal and vertical width in wavenumber space (0.06 and 0.12, respectively) are determined from the standard deviation of the power spectrum calculated for values within 95% of the peak value. The spectrum shown in Figure 4b of the large-amplitude wavepacket at time $t = 200$ is much broader. The horizontal wavenumber is centred about $k_x \simeq 1.0 \pm 0.06$, the width about the peak being comparable to that of the small-amplitude case. However, the vertical wavenumber spectrum is more broadly distributed with mean $k_z \simeq 0.97 \pm 0.47$. The spectrum exhibits two strong peaks near $k_z \simeq 0.7$ and $k_z \simeq 0.3$, and a smaller peak with $k_z \simeq 1.1$. The power spectrum is greater than 0.1 for values of k_z ranging from 0.1 to 1.9. This range is three times larger than the corresponding range in the small-amplitude case. Because the wavenumber spectrum is broader, the frequency spectrum is also broader. Linear theory is used to estimate the frequency of the waves from the wavenumber vector. The frequency of the waves with peak power at $(k_x, k_z) = (1, 0.3)$ is 0.96, at $(k_x, k_z) = (1, 0.7)$ is 0.82, and at $(k_x, k_z) = (1, 1.1)$ is 0.67. Thus, if the background flow, $U(z)$, is not uniform but changes according to equation (7) with U_1 negative, then the proportion of the wavepacket that reflects is expected to be different for large-amplitude and small-amplitude waves. This amplitude dependent behaviour is the result of weakly nonlinear interactions between the waves and the wave-induced mean-flow, otherwise known as the self-acceleration of the waves [8,9].

As shown by Sutherland[7], the wave-induced mean-flow for horizontally periodic internal waves in uniformly strat-

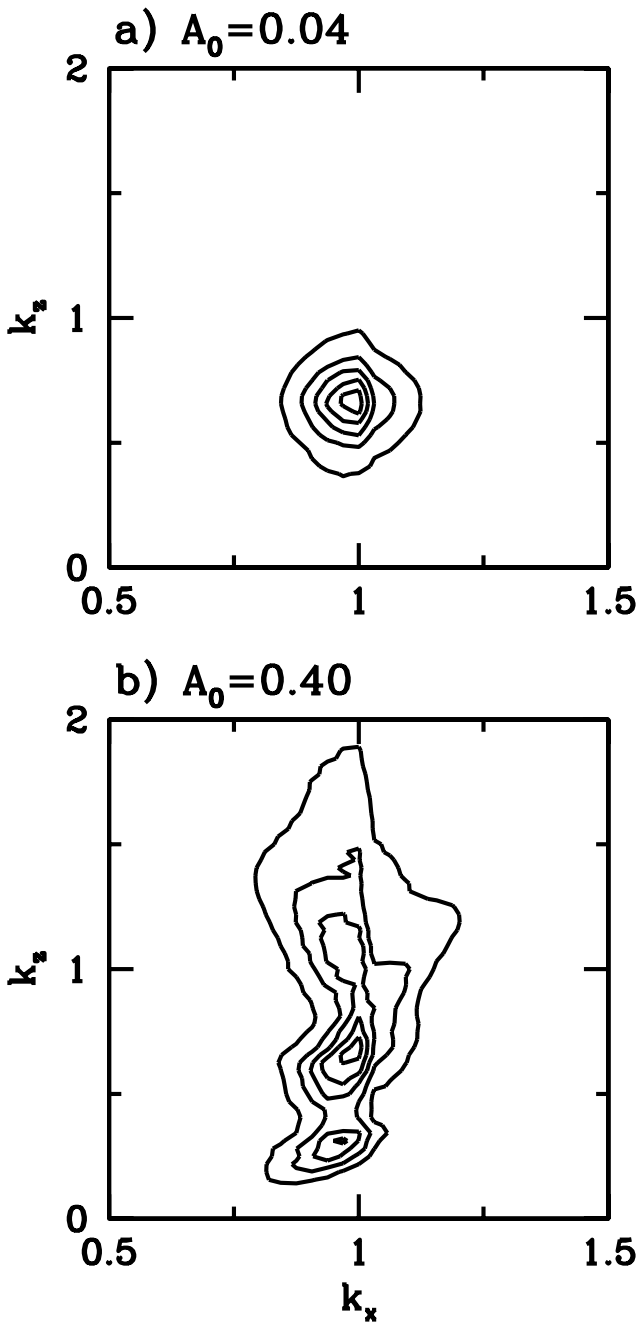

FIG. 4. Normalised power spectra of a) small-amplitude and b) large-amplitude compact wavepackets at time $t = 200$, computed from perturbation density fields shown in Figure 3b and d, respectively. Contours are shown by intervals of 0.2.

ified fluid is given approximately by the mean horizontal wave pseudomomentum[14]:

$$\overline{U} \simeq \mathcal{M} = \overline{\zeta'\xi'}, \tag{8}$$

in which ζ' and ξ' are the perturbation vorticity and vertical displacement fields, respectively. This estimate is accurate to $O({A_0}^3)$. The wave pseudomomentum is well defined for horizontally periodic flows. For compact waves, the effect of self-acceleration is demonstrated by calculating the $\zeta'\xi'$ field and at each point in the field calculating the horizontal average over one wavelength, $\lambda_x = 2\pi$: $\overline{\zeta'\xi'}^{\lambda_x}$. The result is shown in Figure 5 from simulations at time $t = 200$ for a) small-amplitude ($A = 0.04$) and b) large-amplitude ($A = 0.40$) wavepackets in stationary, uniformly stratified fluid. The gray-scale shows the perturbation density field at this time, reproduced from Figures 3b and d. Superimposed on these are contours of $\overline{\zeta'\xi'}^{\lambda_x}$, The undulations in the contours are an artifact of the averaging procedure. Nonetheless, the large-scale features give an adequate representation of where the wave-induced flow is significant. In Figure 5a the contours are shown by intervals of 0.0002, the peak value occurring near the centre of the wavepacket at $(x, z) \simeq (55, -50)$ with value $\overline{U} \simeq 0.001$. In Figure 5b the contours are shown in intervals of 0.005. In this case, there are two peak values occurring near $(x, z) \simeq (55, -50)$ with value $\overline{U} \simeq 0.025$, and near $(80, -30)$ with value $\overline{U} \simeq 0.035$. From linear theory, the group velocity of the initial wavepacket is estimated to be $(c_{gx}, c_{gz}) \simeq (0.27, -0.38)$. Thus, the wave-induced mean flow of the large-amplitude wavepacket is as large as 10% the horizontal group velocity and, therefore, has an arguably significant impact upon the wavepacket evolution.

From the group velocity, the position of the wavepacket at time $t = 200$ is estimated to be at approximately $(54, -51)$. This is comparable with the observed position of the small-amplitude wavepacket, and also with the position of the lower peak value of $\overline{U}$ of the large-amplitude wavepacket. It is interesting to note that the position of the stronger peak value of $\overline{U}$ is consistent with that expected for a wavepacket with the largest horizontal group velocity for which $(k_x, k_z) = (1, \sqrt{2})$ and $(c_{gx}, c_{gz}) \simeq (0.38, -0.27)$. A detailed analysis of the division of an initial large-amplitude wavepacket into parts is currently under investigation, but beyond the scope of this paper.

C PERIODIC INTERNAL WAVES IN A SHEAR FLOW

Here the propagation of a horizontally periodic wavepacket is examined as it propagates downward through a uniformly stratified shear flow. The background flow has zero speed over the depth of the initial wavepacket and has uniform and negative speed at great depths. Because the initial wavepacket has positive horizontal phase speed, the Doppler-shifted frequency of the wavepacket, $\Omega = \omega - c_{px}U$, becomes larger as it propagates downward. If Ω equals the buoyancy frequency $N_0 = 1$ at some depth, then the wavepacket encounters a reflecting level. For small-amplitude internal waves, it is found that the wavepacket is partially reflected from and transmitted across a reflecting level due to transient effects[7].

Figure 6 shows the results of a simulation of a small-amplitude wavepacket, with $A_0 = 0.01$, propagating through fluid in which the background velocity is given by equation (7) with $U_1 = -0.2$. In this case the Doppler-shifted frequency of the wavepacket well below $z = 0$ is $\Omega_1 \simeq 1.02 > N_0$. Therefore, a reflecting level exists near $z = 0$. Figure 6a shows a horizontally offset sequence of

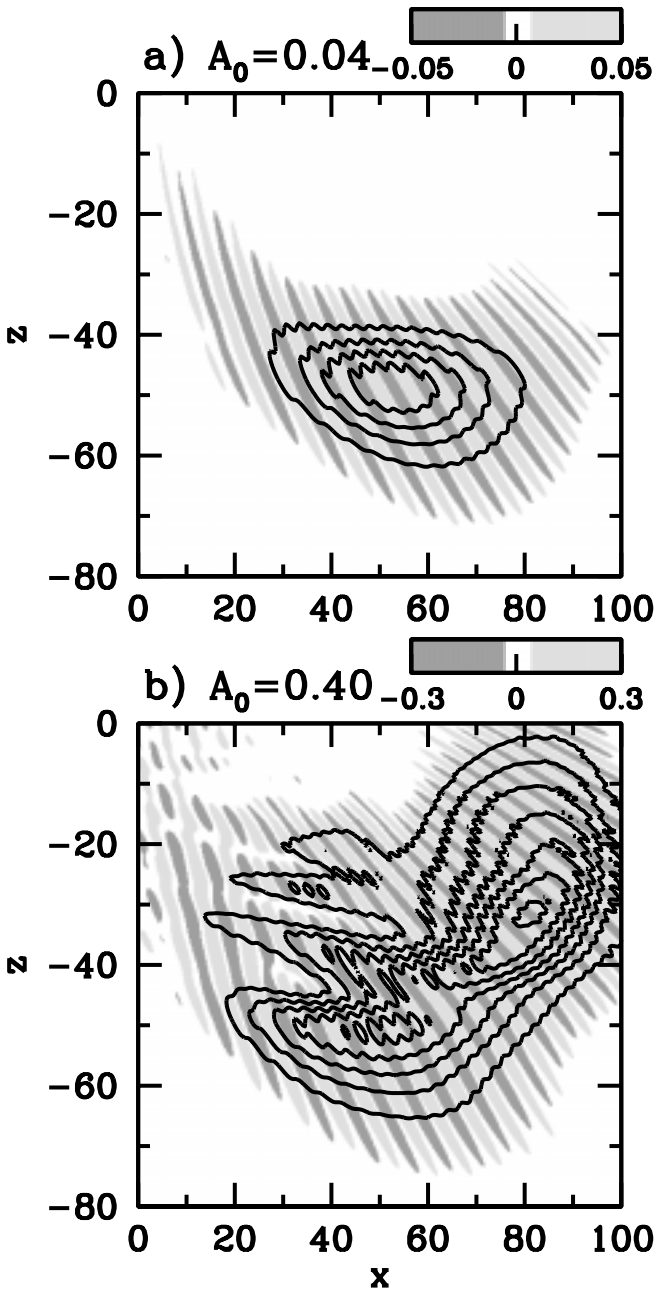

FIG. 5. Contours of $\overline{\zeta'\omega'}^{\lambda_x}$ field (black lines) for a) small-amplitude and b) large-amplitude compact wavepacket in control simulation at time $t = 200$. The contours are superimposed on pertubation density field (gray-scale) which are reproduced from Figure 3b and d, respectively. Contours are shown by intervals of a) 0.0002 and b) 0.005.

profiles of the Reynolds stress, $\tau(z)$. From left to right, the profiles are shown at times $t = 0, 10, \ldots, 200$. Each profile is shown on a scale ranging from -10^{-4} to 4×10^{-5} Initially, τ is negative about a peak centered at $z = 25$. The sign of τ is consistent with the downward transport of forward momentum by the propagating wavepacket. It encounters the reflecting level near $z \simeq 0$ around time $t \simeq 80$ and then proceeds to split into two wavepackets, one that continues to propagate downward with an associated negative Reynolds stress ($\tau(z) < 0$ for $z < 0$), and one that propagates upward with an associated positive Reynolds stress ($\tau(z) > 0$ for $z > 0$). Figure 6b shows the perturbation density field at $t = 200$ in this simulation. The contours in the diagram range between -0.02 and 0.02. The diagram shows two wavepackets, which can be distinguished from the tilt of the phase lines above and below $z = 0$. The right and downward tilt of the waves below $z = 0$ is consistent with their expected downward propagation. By calculating the position of the centroid of the perturbation kinetic energy associated with the wavepacket with negative Reynolds stress, the wavepacket is found to be centred about $z \simeq -33.7$ with width 7.8. The right and upward tilt of the waves above $z = 0$ is consistent with upward propagation. These waves are centered about $z \simeq 27.3$ with width 10.0.

For comparison, a simulation is performed with the same initial background flow but for a large-amplitude wavepacket with $A_0 = 0.10$. As in Figure 6, Figure 7a shows a sequence of profiles of $\tau(z)$, each profile shown on a scale ranging from -10^{-2} to 6×10^{-3}. As in the small-amplitude case, the wavepacket encounters the reflecting level near $z = 0$ and splits into a transmitted, downward propagating and reflected, upward propagating wavepacket. By comparison, the vertical width of both wavepackets at late times is moderately smaller. Figure 7b shows the perturbation density field associated with the waves at time $t = 200$. The contours range from -0.25 to 0.25. As before, it is found that the tilt of the phase lines below $z = 0$ is downward and to the right. This downward propagating wavepacket is centered about $z \simeq -34.0$ with width 7.2. The upward propagating wavepacket above $z = 0$ is centered about $z \simeq 32.2$ with width 6.3.

Nonlinear effects act to reduce the width of the wavepacket and to increase its vertical group velocity. As will be shown in section IV, nonlinearity also acts to increase or decrease the proportion of the wavepacket that is reflected.

D COMPACT INTERNAL WAVES IN A SHEAR FLOW

As discussed above, horizontal and vertical wave dispersion can be enhanced for large-amplitude compact wavepackets due to wave self-acceleration. When a compact wavepacket encounters a reflecting level, the superposition of the incident and reflected wavepackets effectively increases the amplitude of the waves and thus the dispersion of the waves is further enhanced. Here the effect of this dispersion upon the structure of the reflected and transmitted waves is qualitatively examined.

Figure 8 shows the results at time $t = 200$ of two simulations of the propagation of a small- and large-amplitude compact wavepackets. In both cases the horizontal width is $\sigma_x = 10$. As in the simulations of horizontally periodic internal waves discussed above, the background flow speed is given by equation (7) with $U_1 = -0.2$. Thus the Doppler-shifted frequency of the wavepacket well below $z = 0$ is $\Omega \simeq 1.02$, and so a reflecting level exists

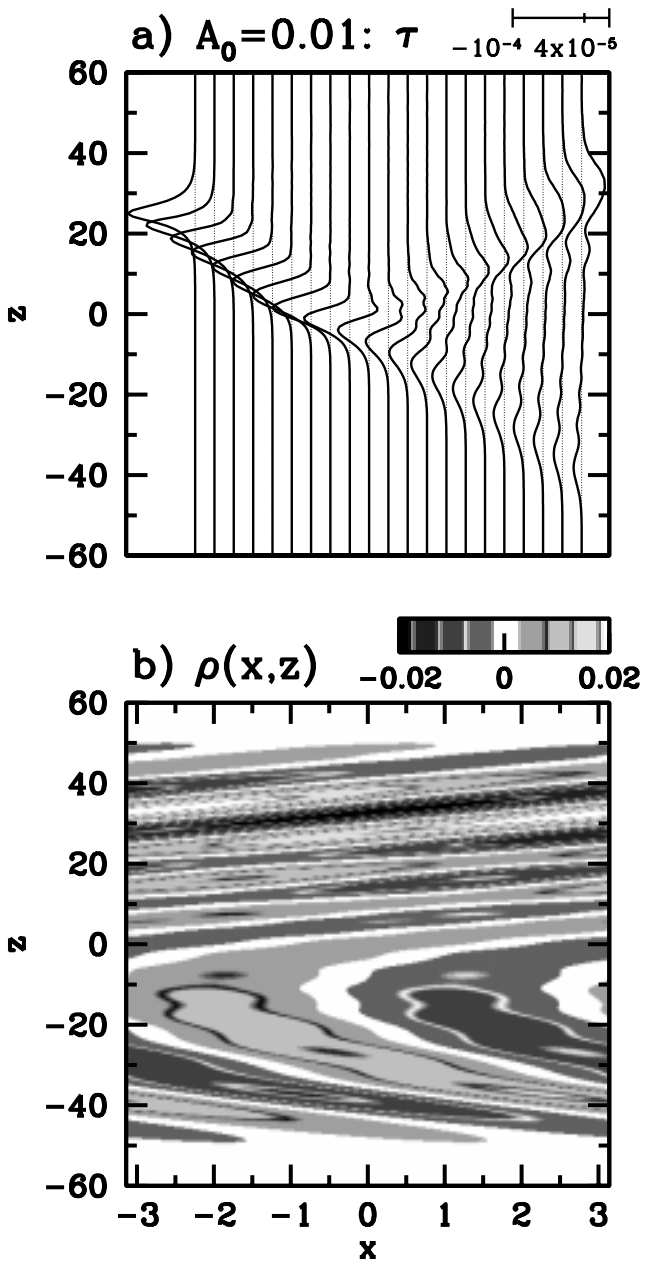

FIG. 6. In a) a sequence of offset Reynolds stress profiles at times $t = 0, 10, \ldots 200$, and in b) the perturbation density field at $t = 200$ from a simulation of small-amplitude horizontally periodic wavepacket incident upon a reflecting level.

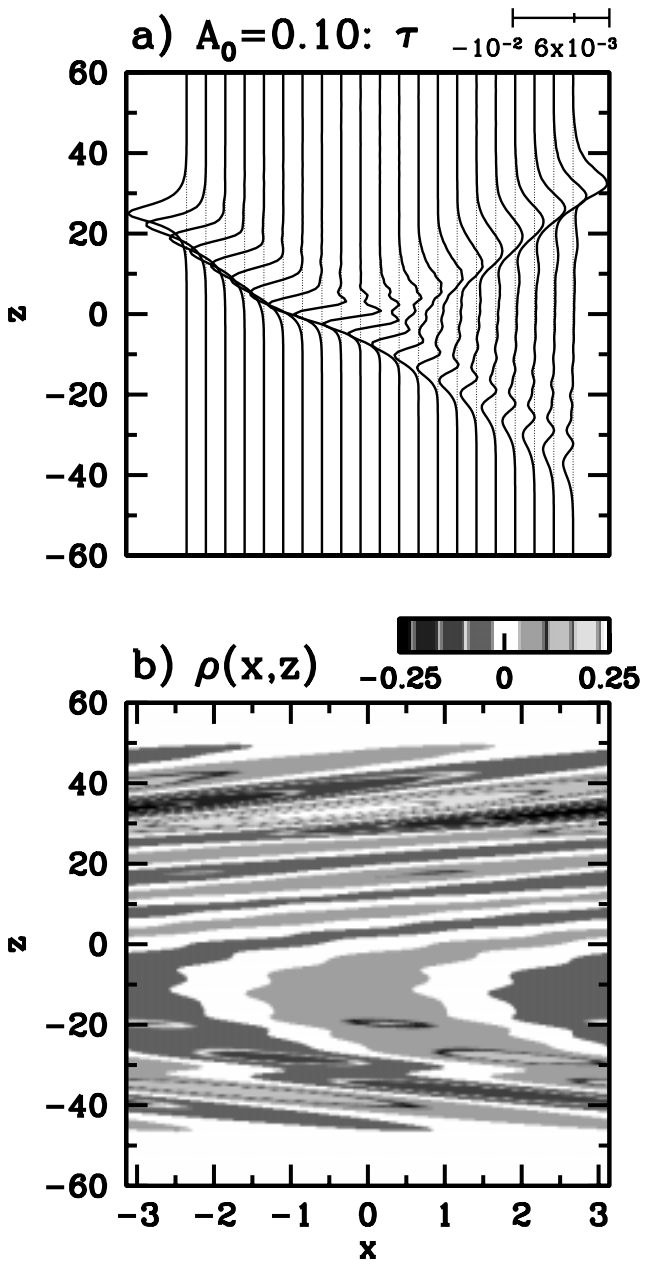

FIG. 7. As in Figure 6 but for a large-amplitude periodic wavepacket.

near $z = 0$. Figure 8a shows the Reynolds stress profile at $t = 200$ for a simulation of a small-amplitude wavepacket with $A_0 = 0.04$. Figure 8b shows the corresponding perturbation density field over the same vertical extent. Only a fraction of the horizontal extent of the computational domain is shown. Contours range between -0.05 and 0.05. Due to the horizontal dispersion of the wave, the peak perturbation density is less than half that of the peak value at time $t = 0$.

The wavepacket below $z = 0$ has right and downward-tilting phase lines, and the Reynolds stress is negative over its vertical extent. These characteristics are consistent with a downward propagating wavepacket. From its perturbation kinetic energy profile at this time, the downward propagating wavepacket is found to be centred about $z \simeq -40.0$ with width 10.3. Consistent with the properties of upward propagating internal waves, the wavepacket above $z = 0$ has right and upward-tilting phase lines, and its associated Reynolds stress is positive. It is centred about $z \simeq 28.3$ with width 9.7.

Figure 8c shows the Reynolds stress profile for a simulation of a large-amplitude wavepacket with $A_0 = 0.40$. Figure 8d shows the corresponding perturbation density field, with contours ranging from -0.3 to 0.3. As in the case with $A_0 = 0.04$, the diagrams show the transmis-

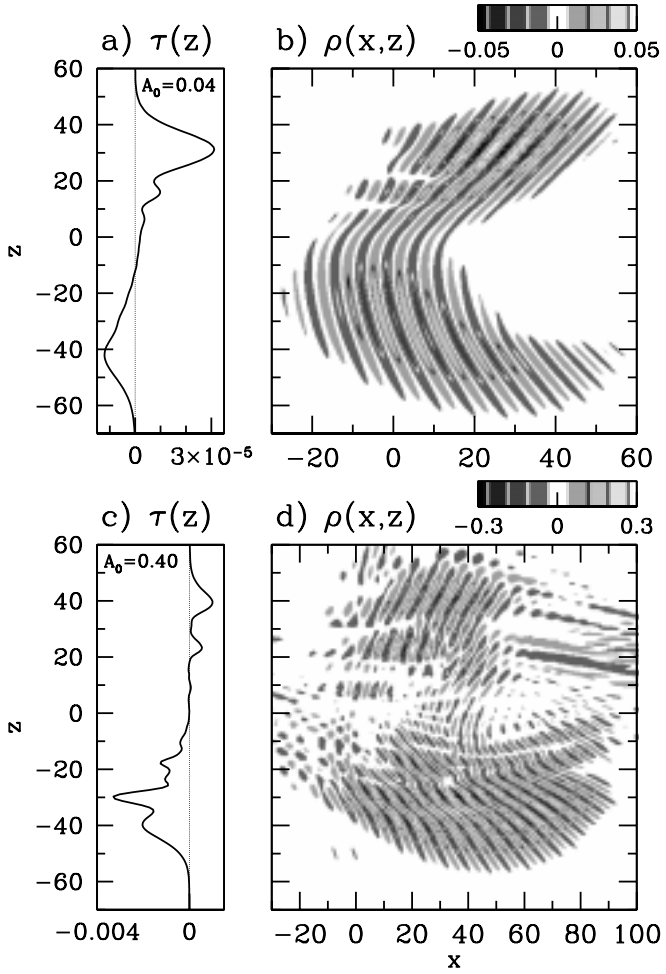

FIG. 8. The a) Reynolds stress profile and b) perturbation density field at time $t = 200$ from simulation of a small-amplitude horizontally compact wavepacket of width $\sigma_x = 10$. Diagrams c) and d) are the corresponding plots from a simulation of a large-amplitude wavepacket.

sion and reflection of the wavepacket across a reflecting level near $z = 0$. In this case, however, the structure and relative amplitude of the wavepackets are significantly different. Although initially the amplitude of the large-amplitude wavepacket is ten times larger than that of the small-amplitude wavepacket, at time $t = 200$ the amplitude is only 6 times larger.

The horizontal extent of the wavepacket is much broader. Below $z = 0$ its half width is approximately 25, compared with that of the small-amplitude wavepacket which is approximately 17. The Reynolds stress associated with the downward propagating wavepacket has multiple peaks and the magnitude of the momentum flux associated with it is significantly larger than the magnitude of the momentum flux of the upward propagating wavepacket above $z = 0$. The centroid of the wavepacket is at $z \simeq -32.1$ with width 9.9, which is not as deep as its counterpart in the simulation of the small-amplitude wavepacket (Figure 8b). Thus the average vertical speed of propagation of the wavepacket below $z = 0$ is smaller in the large-amplitude case. The centroid of the upward propagating wavepacket above the

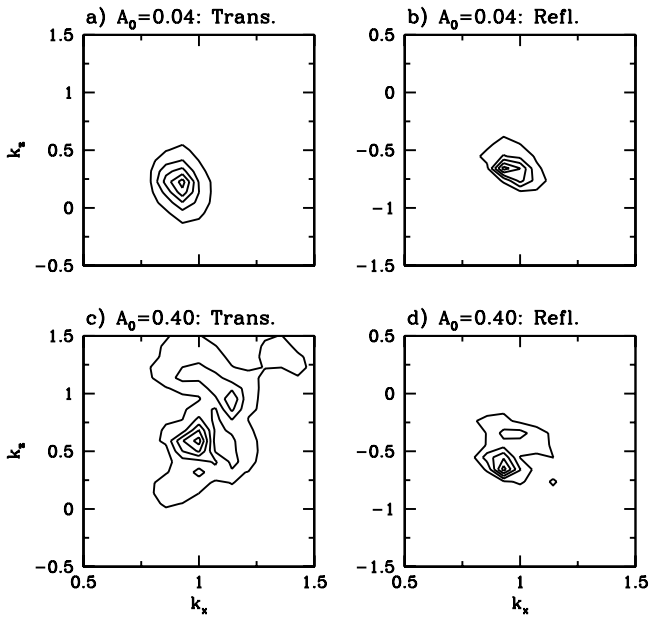

FIG. 9. Normalised power spectra of a) transmitted and b) reflected small-amplitude wavepacket computed from perturbation density fields shown in Figure 8b. Diagrams c) and d) show the corresponding plots computed for a large-amplitude wavepacket, the perturbation density field of which is shown in Figure 8d.

reflecting level is at $z \simeq 36.5$ with width 8.4. This is significantly higher than the depth of its small-amplitude counterpart, and thus the average vertical speed of propagation of the reflected wavepacket is larger in the large-amplitude case.

The normalised power spectrum of the transmitted and reflected wavepackets is calculated from the perturbation density field as described in section IIIB. From simulations at time $t = 200$ when the transmitted, downward propagating and the reflected, upward propagating wavepackets are sufficiently spatially separated, the power spectrum is calculated for the field below and above $z = 0$, respectively. Figure 9 shows the power spectrum for the simulations of the small ($A = 0.04$) and large ($A = 0.40$) amplitude wavepackets at time $t = 200$. The corresponding perturbation density fields are shown in Figure 8b and d, respectively. In each case the contours are shown in intervals of 0.2 ranging from 0.1 to 0.9. Figure 9a shows the power spectrum of the transmitted small-amplitude wavepacket. The peak power occurs at wavenumber $(k_x, k_z) \simeq (0.96 \pm 0.05, 0.27 \pm 0.14)$. From linear theory, this corresponds to a Doppler-shifted frequency of $\Omega \simeq 0.96$, close to the background buoyancy frequency $N = 1$. The horizontal wavenumber is 4% smaller than that of the wavepacket at time $t = 0$. Figure 9b shows the power spectrum of the reflected small-amplitude wavepacket. For these waves, the power is sharply peaked about $(k_x, k_z) \simeq (0.96 \pm 0.06, -0.63 \pm 0.09)$. The corresponding frequency is comparable with the frequency of the initial wavepacket.

Figure 9c shows the power spectrum of the transmitted large-amplitude waves. The peak in the power spectrum occurs for wavenumbers about $(k_x, k_z) \simeq (1.04 \pm 0.05, 0.63)$. The width of the vertical wavenumber spectrum is much broader than the small-amplitude case. However, the horizontal wavenumber spectrum remains sharply peaked. The weighted mean power occurs for $k_z \simeq 0.90$ with standard deviation 0.33. The power spectrum of the reflected large-amplitude wavepacket is shown in Figure 9d. Here the peak power occurs about $(k_x, k_z) \simeq (0.96 \pm 0.05, -0.63)$, and the weighted mean power occurs for $k_z \simeq -0.48$ with standard deviation 0.16.

Thus, while nonlinear effects do not act to change the horizontal wavenumber spectrum significantly, the vertical wavenumber spectrum and the frequency varies greatly. It is interesting to note that for the large-amplitude wavepacket, the absolute values of the peak vertical wavenumbers of the reflected and transmitted wavepackets are comparable and close to the value of the vertical wavenumber of the initial wavepacket.

In both the small- and large-amplitude cases incident upon a region where $\Omega > N$, the power associated with the transmitted wavepacket is significant only for positive values of k_z. That is, the waves are not evanescent, but downward propagating. For small-amplitude waves, the reflecting level acts as a filter that removes the proportion of the wavepacket associated with Doppler-shifted frequencies larger than N. For large-amplitude waves, this filtering acts in conjunction with nonlinear effects that distort the spectrum of the initial wavepacket.

IV REFLECTION COEFFICIENTS

To quantify the degree to which incident waves reflect, the reflection coefficient, $\mathcal{R}$, is calculated, this acting as a measure of the proportion of the wavepacket that is propagating upward at time $t = 200$. Explicitly, $\mathcal{R}$ is defined as the ratio of the integral of the perturbation kinetic energy above $z = 0$ to the integral of this energy over the whole domain. Though not shown here, the reflection coefficient has also been calculated in terms of the total energy (*i.e.* the perturbation kinetic and available potential energy) and, for horizontally periodic waves, in terms of the wave pseudomomentum. The calculated reflection coefficient is approximately the same in each case. Plots of the evolution of the reflection coefficient in time (not shown here) demonstrate that $\mathcal{R}$ changes by less than 5% between times $t = 150$ and 200.

Figure 10 shows the reflection coefficient of horizontally periodic internal waves as a function of the ratio of the Doppler-shifted frequency of the wavepacket in the deep fluid, $\Omega_1 = \omega - k_x U_1$, to the buoyancy frequency $N_0 = 1$. If $\Omega_1/N_0 > 1$, then the initial wavepacket encounters a reflecting level near $z = 0$. From linear theory, plane periodic (*i.e.* monochromatic) internal waves are expected to reflect entirely from this level, so that $\mathcal{R} = 1$. Likewise, if $\Omega_1/N_0 < 1$, from linear theory plane periodic waves are expected to transmit entirely so that $\mathcal{R} = 0$. However, because the vertical extent of the wavepackets in the simulations is finite the waves are not monochromatic. Indeed, for a small-amplitude wavepacket with $A_0 = 0.01$ (solid line), the reflection coefficient is significantly less than 1 for $1 < \Omega_1/N_0 < 1.1$, and $\mathcal{R} \gg 0$ for $0.9 < \Omega_1/N_0 < 1$. Sutherland[13] has shown that the form of this curve is well predicted by linear theory that takes into account the initially broad power spectrum of the simulated waves.

If the initial wavepacket is of large amplitude, the proportion of the initial wavepacket that is reflected is less than that predicted by linear theory if $\Omega_1/N_0 > 1.04$. If $\Omega_1/N_0 < 1.04$, the proportion of the initial wavepacket that is transmitted is greater than that predicted by linear theory.

As shown above, nonlinear effects significantly broaden the spectrum of a wavepacket that is horizontally compact. Figure 11 shows the reflection coefficients as a function of Ω_1/N_0 for simulations of horizontally compact wavepackets. In a) the reflection coefficients are shown for simulations of wavepackets with horizontal width $\sigma_x = 10$ and a range of amplitudes from $A_0 = 0.04$ (solid line), to $A_0 = 0.40$ (dot-dashed line), as indicated on the diagram. When the initial wavepacket is of small amplitude (*e.g.* $A = 0.04$), the reflection coefficient as a function of Ω_1/N_0 is similar to that for horizontally periodic internal waves. The curve agrees well with that predicted by linear theory (not shown).

Due to the dispersion of compact wavepackets, the amplitude decreases rapidly in time from its initial value. Thus for $A_0 < 0.10$, the amplitude of the wave at time $t = 200$ is so small that the curve $\mathcal{R}(\Omega_1/N_0)$ differs insignificantly from that predicted by linear theory. For larger values of the initial amplitude, enhanced transmis-

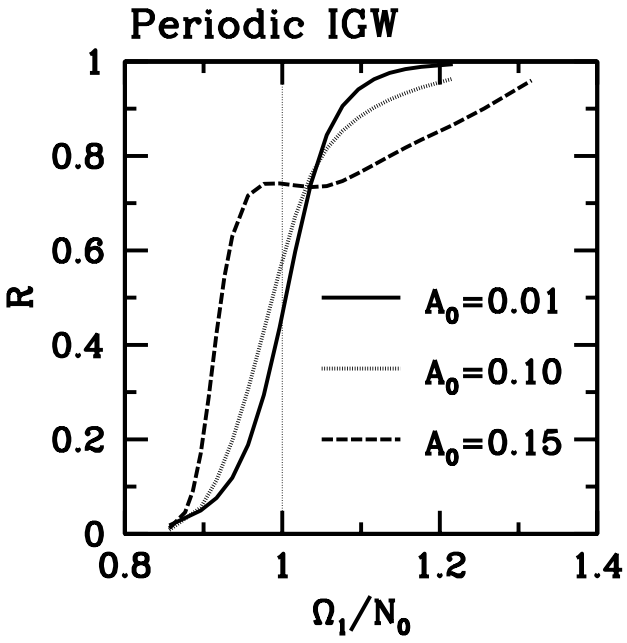

FIG. 10. The reflection coefficient as a function of Ω_1/N_0 for periodic wavepackets of amplitude $A_0 = 0.01$ (solid line), $A_0 = 0.10$ (short-dashed line) and $A_0 = 0.15$ (long-dashed line).

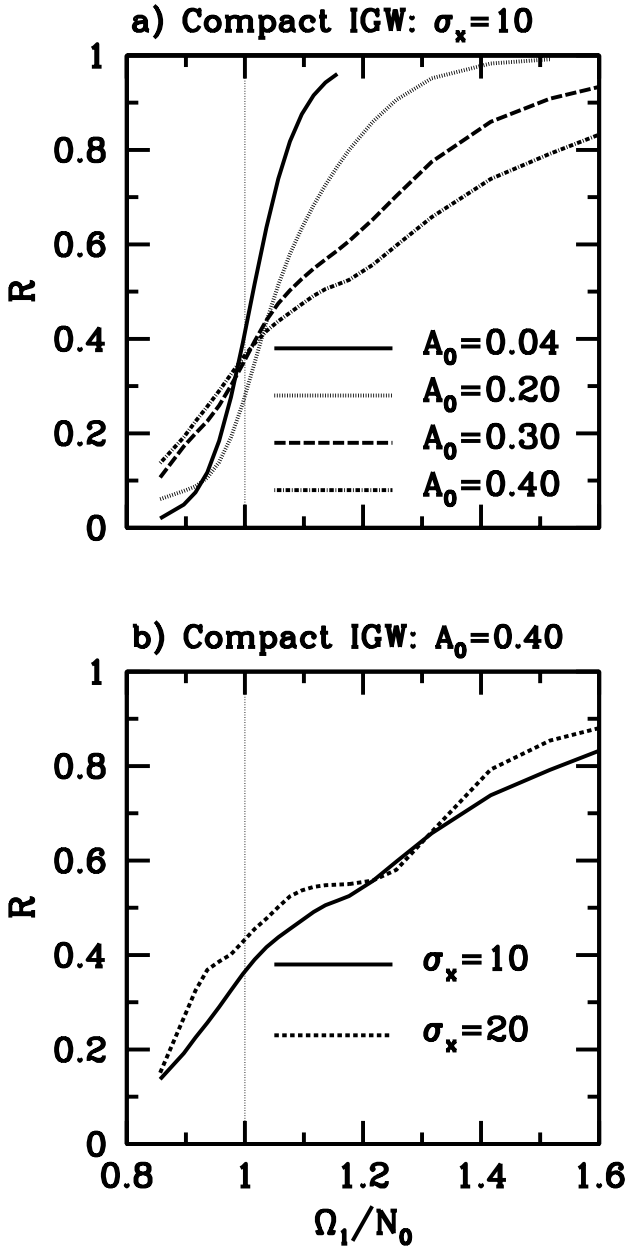

FIG. 11. The a) reflection coefficient as a function of Ω_1/N_0 for compact wavepackets of amplitude $A_0 = 0.04$ (solid line), $A_0 = 0.20$ (short-dashed line) and $A_0 = 0.30$ (long-dashed line), and $A_0 = 0.40$ (dash-dotted line). b) Reflection coefficient for large-amplitude compact wavepacket with $A_0 = 0.40$ and width $\sigma_x = 10$ (solid line) and $\sigma_x = 20$ (dashed line).

sion of the wavepacket occurs for $\Omega_1/N_0 > 1$. Indeed, $\mathcal{R}$ is significantly less than 1 over a much greater range than that for horizontally periodic wavepackets. For example, if $A_0 = 0.40$ and $\Omega_1/N_0 = 1.82$ ($U_1 = -1.0$), the reflection coefficient is $\mathcal{R} = 0.89$ for a compact wavepacket with $\sigma_x = 10$, whereas $\mathcal{R}$ is negligibly different from 1 for a periodic wavepacket of comparable amplitude at time $t = 200$. For $\Omega_1/N_0 < 1$, the reflection of the incident wavepacket is enhanced, though to a lesser degree for compact wavepackets than for periodic wavepackets.

Figure 11b compares the reflection coefficients for simulations of large-amplitude wavepackets ($A_0 = 0.40$) with horizontal widths $\sigma_x = 10$ and 20. The plot shows that the reflection coefficient is generally larger for a wavepacket of double the width over the calculated range $0.86 < \Omega_1/N_0 < 1.82$. This result is consistent with the expectation that in the limit of compact wavepackets of very large horizontal extent, the reflection coefficient should approach that for horizontally periodic waves. Simulations of wavepackets of horizontal extent significantly larger than $\sigma_x = 20$ have not been possible due to limitations in the speed and memory of the computational resources available.

V DISCUSSION AND CONCLUSIONS

Numerical simulations have demonstrated that the amplitude and horizontal extent of a wavepacket are significant factors in determining the dynamics of internal waves incident upon a reflecting level. In particular, this work demonstrates that a significantly greater proportion of incident internal waves may be transmitted above a reflecting level than predicted by linear theory. Compared with horizontally periodic waves, an even greater proportion of the incident wavepacket is transmitted for a wavepacket that is horizontally compact but whose horizontal extent encompasses many wavelengths. For example, linear theory predicts almost 100% reflection of a wavepacket with amplitude $A_0 = 0.40$ that propagates across a shear flow into a region where its Doppler shifted frequency is 20% greater than the background buoyancy frequency. (For reference, the maximum vertical displacement of this wavepacket initially is $A_{\Delta z} \simeq 1$, about 16% of the horizontal wavelength.) In fact, approximately 50% of a wavepacket with this amplitude is transmitted below the reflecting level and where it continues to propagate.

At present it is not obvious how the results presented here might be efficiently employed in a general circulation model. In these models and in analytic theories applied to understanding the impact of internal waves upon the large-scale circulation of the atmosphere and ocean, linear theory is frequently employed to estimate at which vertical levels incident internal waves might break or reflect. This approach is beneficial in part because it is easily adapted to speedy computation in numerical models. In many oceanographic and atmospheric circumstances, internal waves have been observed with amplitudes large enough that nonlinear effects play a significant role. The results presented here demonstrate, however, that this methodology should be applied with caution when modelling the dynamics of non-hydrostatic large-amplitude internal waves.

It is worthwhile commenting upon the possibility of applying weakly nonlinear theory to elucidate further the results presented here. Weakly nonlinear evolution equations have been developed by Smith[15] to model the growth in amplitude of surface waves near caustics, and Peregrine and Smith[16] have modelled the weakly nonlinear behaviour near caustics of dispersive waves in general. The resulting equations, which have the form of a Nonlinear Schrödinger

(NLS) equation, require that the background varies slowly on a scale comparable with the wavelength of the waves. This is not the case for the waves studied here: in order to demonstrate the steady propagation of transmitted and reflected waves, the simulations have been set up so that the background is uniform well above and well below a localised region within which the background flow varies over a length-scale comparable with the vertical wavelength of the wavepacket.

Weakly nonlinear theory has been applied to examine the resonant over-reflection of internal waves at a critical level (where the phase speed of the wave equals the speed of the background flow) in a thin shear layer[17]. However, these results cannot easily be extended to examine the reflection of waves from a reflecting level because the incident waves cannot not couple with an unstable mode of the background flow; the phase speed of the incident waves must lie outside the range dictated by Howard's semicircle theorem[18].

In order to adapt existing weakly nonlinear theories of waves near caustics to the study of reflecting internal waves, a straightforward first step would be to run a new series of numerical simulations modelling the behaviour of internal waves propagating in constant, but weak shear. In these simulations, total reflection of the waves, independent of the initial wavepacket amplitude, is anticipated. However, weakly nonlinear effects would act to shift the vertical level at which the waves reflect. This research is currently under progress.

[1]F. P. Bretherton, "Gravity waves in shear," Quart. J. Roy. Meteorol. Soc. **92**, 466 (1966).

[2]K. B. Winters and E. A. D'Asaro, "Three-dimensional wave instability near a critical level," J. Fluid Mech. **272**, 255 (1994).

[3]P. N. Lombard and J. J. Riley, "On the breakdown into turbulence of propagating internal waves," Dyn. Atmos. Ocean **23**, 345 (1996).

[4]M. J. Lighthill, *Waves in Fluids* (Cambridge University Press Cambridge, England, 1978).

[5]W. Blumen, "Reflection of hydrostatic gravity waves in a stratified shear flow. part i: Theory," J. Atmos. Sci. **42**(21), 2255 (1985).

[6]S. D. Eckermann, "Influence of wave propagation on the Doppler spreading of atmospheric gravity waves," J. Atmos. Sci. **54**, 2554 (1997).

[7]B. R. Sutherland, "Internal gravity wave radiation into weakly stratified fluid," Phys. Fluids **8**, 430 (1996).

[8]R. H. J. Grimshaw, "Nonlinear internal gravity waves and their interaction with the mean wind," J. Atmos. Sci. **32**, 1779 (1975).

[9]D. C. Fritts and T. J. Dunkerton, "A quasi-linear study of gravity-wave saturation and self-acceleration," J. Atmos. Sci. **41**, 3272 (1984).

[10]A. Eliassen and E. Palm, "On the transfer of energy in stationary mountain waves," Geofys. Publ. **22**, 1 (1961).

[11]D. G. Andrews and M. E. McIntyre, "Planetary waves in horizontal and vertical shear: The generalized Eliassen-Palm relation and the mean flow acceleration," J. Atmos. Sci. **33**, 2031 (1976).

[12]W. D. Smyth and W. R. Peltier, "The transition between Kelvin-Helmholtz and Holmboe instability: An investigation of the overreflection hypothesis," J. Atmos. Sci. **46**(24), 3698 (1989).

[13]B. R. Sutherland, "The dynamic excitation of internal gravity waves in the equatorial oceans," J. Phys. Oceanogr. **26**, 3214 (1996).

[14]J. F. Scinocca and T. G. Shepherd, "Nonlinear wave-activity conservation laws and Hamiltonian structure for the two-dimensional anelastic equations.," J. Atmos. Sci. **49**, 5 (1992).

[15]R. Smith, "Giant waves," J. Fluid. Mech. **77**, 417 (1976).

[16]D. H. Peregrine and R. Smith, "Nonlinear effects upon waves near caustics," Proc. R. Soc. Lond. A **292**, 341 (1979).

[17]R. H. J. Grimshaw, "Resonant over-reflection of internal gravity waves from a thin shear layer," J. Fluid Mech. **109**, 349 (1981).

[18]L. N. Howard, "Note on a paper by John W. Miles," J. Fluid Mech. **10**, 509 (1961).